Structural and Optical Analysis of Green-Synthesized ZnO Nanoparticles

Firas. H.Ibrahim and Olfat. A. Mahmood
Department of Physics, College of Science, University of Diyala, 32001 Baqubah, Iraq
firas.haider1982@gmail.com, olfat@udiyala.edu.iq,

Keywords: Calcination Temperature, Zno Nps, Leaves of Crocus Sativus L, Tree Extract, Green Synthesis.

Abstract: Extracts from the leaves of Crocus sativus L. (CS) were used to synthesize zinc oxide (ZnO NPs) nanoparticles. It has been studied on the properties of ZnO NPs nanoparticles using CS tree extracts, utilising several characterization techniques. The selected plant CS demonstrated findings from both FTIR and UV-visible spectroscopies, indicating it as a preferable alternative for the levels of CS ZnO NPs. The UV-visible spectra of CS tree leaf extracts exhibited a distinct absorption peak at 274 nm. Absorption peaks at 345 nm and 375 nm, characteristic of zinc oxide nanoparticles. Field emission scanning electron microscope (FESEM) data analysis of the particles size before and after calcination from 34.32 nm to 61.52 nm respectively showed that the calcination temperatures significantly affected the orientation, shape and dimensions of the ZnO NPs nanoparticles synthesized by the green synthesized. An FT-IR spectroscopy study reveals an absorption peak indicative of Zn–O bonding within the range of 400 to 600 cm^{-1}.The XRD findings indicate that the ZnO NPs nanoparticles possess hexagonal wurtzite crystal structures, and that the principal diffraction peaks (100), (002), and (101) exhibit variations in intensity with differing heating temperatures. The average crystal size of synthesised grains was determined to be 22.7 nm for ZnONPs without calcination and 31.5 nm for ZnONPs subjected to calcination at 450 °C. The results and characteristics indicate that ZnO NPs nanoparticles calcined at 450°C exhibit improved quality compared to those synthesised without thermal treatment. The calcined ZnO NPs nanoparticles exhibited an increase in crystallite size, alongside higher optical purity and a shift in the absorption peak from 345 nm to 375 nm, indicating improved crystallinity.

1 INTRODUCTION

Nanotechnology is a multidisciplinary field focused on the creation of innovative materials at the nanoscale (1–100 nm), applicable across diverse domains [1]. At the nanoscale, materials exhibit enhanced characteristics like increased surface area, thermal conductivity, charge, dimensions, morphology, surface topology, and crystal structure, facilitating their integration into biomedical and biotechnological fields [2], [3]. Nanoparticles (NPs) can be synthesized by several techniques, including chemical, physical, and biological approaches. The previous chemical and physical procedures employed hazardous materials and required extreme conditions, including temperature, energy, and pressure, often resulting in dangerous by-products [2], [4]. Consequently, interest in biological techniques and green nanotechnology has intensified. Green nanotechnology refers to an environmentally benign approach to synthesizing nanomaterials by minimizing or eliminating the use of hazardous substances in the manufacturing process [5]. Recently, several nanoparticles have been synthesized using environmentally friendly technologies, including silver, gold, copper, copper oxide, zinc oxide, selenium, and others, which are incorporated into diverse biological activities [6], [7]. Biogenic or green-synthesized nanoparticles present a viable alternative as antibacterial and anticancer agents, providing safer, more targeted, and cost-effective options for pharmaceuticals or drug delivery vehicles [8]. Metal oxide nanoparticles are considered superior to other nanoparticles owing to their distinctive physical, chemical, and biological properties [9]. ZnO nanoparticles, known for their remarkable piezoelectric, optoelectronic, pyroelectric, semiconducting, catalytic, and antimicrobial properties, are among them. Nanotechnology amalgamates physics and chemistry to develop nanoscale materials possessing distinctive optical and catalytic characteristics [10], [11]. The

saffron plant (Crocus sativus L.) is abundant in phenolic compounds and flavonoids, rendering it an efficient bio-reductant and stabilizer for ZnO nanoparticles. This green synthesis process has benefits including cost-effectiveness, simplicity of manufacturing, and less environmental toxicity relative to traditional approaches [12]. The aim of this comprehensive analysis and comparison is to provide a comprehensive understanding of the synthesis of zinc oxide nanomaterials using saffron leaf extract. Additionally, the study aims to assess the impact of the plant extract and calcination method on the crystal structure, particle size, and spectral properties of the nanoparticles, and provide recommendations for their potential applications in the environmental and medical fields.

2 EXPERIMENTAL PROCEDURES

2.1 Chemical Materials

Merck (India) provided zinc sulphate Zn SO_4 Merck-98% and all other chemicals and solvents used in the study. Saffron (Crocus sativus L) was supplied from Mashhad, Reza Farm, Iran. This plant was collected and dried there. The alcoholic extract of zinc nanoparticles was prepared in the laboratory of the University of Diyala.

2.2 Preparation of Extract Crocus Sativus L

The saffron leaves were cleaned, washed several times, and left to dry at room temperature for 3 days. After drying, the leaves were grinding into a fine powder by passing them through a blender. 5 grams of saffron powder were added to a mixture of 20% absolute ethanol C_2H_5OH, 65% methanol CH_3OH, and 15% distilled water in a flask and heated at 70°C for less than an hour. The mixture was filtered using Whatman No. 1, cooled and a portion was taken for analysis.

2.3 Preparation of Zinc Oxide Nanoparticles from Zinc Sulphate.

Two grams of zinc sulphate were dissolved in 100 milliliter of distilled water to create an aqueous solution. 10 ml of a 20% alcoholic extract of saffron (Crocus sativus) was incrementally added to the mixture and left to stir constantly with a stirrer. The mixture was heated to 70°C. Pure sodium hydroxide NaOH (1 M) was then added to the mixture in a 1:2 ratio with continuous stirring to neutralise the acidity. The mixture was left at room temperature without stirring until the next day to react in a flask. The precipitate was subsequently isolated from the filtrate using a centrifuge at 6,000 rpm for 15 minutes. The precipitate was then washed several times using distilled water and ethanol. The precipitate was taken and dried in an electric oven at 60°C for about 48 hours and ground using a laboratory mill to obtain a dry powder. Then, a portion of this powder was heated in an oven at 450 degrees Celsius, and samples were stored in glass containers for analysis and comparison of the powder before and after calcination.

2.4 Characterization of ZnO Nps

The Shimadzu UV-Vis – UV-1900 (Shimadzu, Japan) was employed to assess ultraviolet-visible (UV-Vis) absorption spectra within the 200–800 nm range and verify the synthesis of zinc oxide nanoparticles. Fourier Transform-Infrared (FT-IR) measurements in the 400–4000 cm^{-1} range, conducted with an FTIR – Frontier (PerkinElmer, USA), revealed the presence of extract Crocus sativus L-mediated ZnONPs. An apparatus named XRD–AERIS (Malvern Panalytical, Netherlands) was employed to conduct an X-ray diffraction investigation to help clarify the crystalline structure of nanoparticles. The apparatus is equipped with an X-ray generator that emits Cu Kα radiation at 40 kV, with a wavelength of 1.5406 Å. The dimensions and the morphology of the nanoparticles was investigated with a field emission scanning electron microscope (FESEM – Inspect™ F50 (FEI Company, USA)).

3 RESULTS AND DISCUSSIONS

3.1 Characterization of Synthesized ZnONPs

The characterization of biologically synthesized zinc oxide nanoparticles was conducted using FESEM, FT-IR, UV-VIS, XRD, and Energy-Dispersive X-ray Spectroscopy) EDX (techniques. The Field Emission Scanning Electron Microscope) FESEM (images of ZnO NPs nanoparticles reveal the presence of zinc particles, which are uniformly distributed in certain areas while exhibiting clustering in others. The EDX scan revealed the presence of other metals besides zinc as in the Figure 1c. The many metals seen in

EDX are believed to be inherent to the plant's structure [13]. Showed that the morphology of ZnO NPs nanoparticles, synthesized using extracts from the flowers of the Crocus sativus L plant, an irregular and almost spherical shape [14]. As demonstrated by FESEM images Figure 1a. In Figure 2b, the oxide nanoparticles were subjected to calcination at 450 degrees Celsius. The crystallization of the particles was observed, revealing a notable variation in form and size Similar results were detected with [15]. The particle size histogram Figure 1b, 2b was produced from FESEM images utilising ImageJ software, as outlined in prior research [16]. The histogram exhibits a wide size distribution, with an average particle size of (34 ± 9 nm) prior to calcination, which increases to (61.52 ± 11nm) following calcination at 450 degrees Celsius. The morphology and dimensions of zinc oxide nanoparticles augment with elevated calcination temperatures [17]. The reason for the large grain size is that calcination at high temperature causes the grains to continue to grow and merge with each other [18]. This work provides valuable insights on the calcination temperature of the end product of ZnO NPs nanoparticles. Figure 2a illustrates that when the calcination temperature rises, it significantly influences the deagglomeration of the ZnO NPs nanoparticles However, more spherical and uniform. Similar results were [19].

3.2 XRD Studies

The XRD pattern of green-synthesized ZnO NPs is used to determine the crystallinity and average grain size of the synthesized ZnO NPs nanoparticles from Crocus sativus L extract from saffron leaves shows the crystal structure of ZnO NPs the nanoparticles before calcination.

The peaks in the Figure 3a are at 2θ = 31.70° (100), 34.38° (002), 36.18° (101), 47.46° (102), 56.46° (110), 62.76° (103), 66.22° (200), 67.81° (112), 72.47° (004) and 76.79° (202). The aircraft have a strong correlation with the JCPDS file (JCPDS: 01-079-0207 card ICSD#: 06512) in the Figure 3b Peaks for ZnO NPs synthesized with calcination at 450 °C at2θ = 32.07° (100), 34.47° (002), 36.53° (101), 47.79° (102), 57.17° (110), 63.10° (103), 67.07° (200), 68.49° (112), 72.67° (004) and 77.64° (202), respectively, and the JCPDS file (JCPDS: 01-075-1526 card ICSD#: 031052). This clarifies the hexagonal wurtzite structure corresponding to pure zinc oxide nanoparticles [20], [21]. By using the Debye-Scherrer equation [20].

The average crystal size of synthesized particles was calculated to be 22.7 nm for ZnONPs without calcination and 31.5 nm for ZnONPs (with calcination at 450 °C) The strain values, obtained from the uniform deformation model, varied from 3.3 to 0.06, respectively, as indicated by the Williamson-Hall (W-H) [16]. The broad peaks indicate the decrease in crystallinity. This implies the creation of smaller grain sizes before the calcination. Figure 3a, 3b show that (100), (002), and (101), the main and constant diffraction peaks with variable intensity, present in the XRD peaks before and after calcination, had their intensity changed with the calcination of ZnO NPs nanoparticles at 450 °C congruent with research [15]. The diffraction peaks along the (101) plane were more distinct and significant and in good agreement with another research [22]-[24]. Moreover, the increase in the average crystal size with the increase in calcination temperature results in an augmentation of temperature, which leads to an increase in atomic diffusion, which in turn leads to the formation of nuclei in the phase. As the temperature increases, the grain boundaries are removed, leading to an increase in crystal size; this is further evidenced by the narrowing and intensification of the high peaks, which indicate a larger crystal size [25]. The finger print showed enhancement in the crystallinity of the structure as the temperature was raised up to 450 ◦C. This enhancement in the crystallinity affect significantly on the chemical composition of ZnO NPs [19].

3.3 FT-IR Analysis

Infrared research utilizing Fourier transformation techniques: The functional groups in the saffron extract and the zinc oxide nanoparticles synthesized by the green approach were identified through Fourier transform infrared analysis. The spectrum illustrates the plant extract (depicted in black, CS) and zinc oxide particles (depicted in red). Exhibited a maximum between 3415 and 3390 cm^{-1} attributable to the stretching vibrations of the hydroxyl ion (O-H) [26]. Besides the peaks at 2920–2856 cm^{-1} corresponding to C–H vibrations and those at 1773–1443 cm^{-1} signifying C=C and C=O vibrations, this curve substantiates the presence of phenolic compounds, carbohydrates, and amines in the extract, which may function as reducing and stabilizing agents in the nanoparticle synthesis process[27].As illustrated in Figure 4. The strength of the peaks in the organic zone diminished at 2920–2856 cm^{-1} and 1708–1443 cm^{-1}. The integration of zinc oxide into the extract suggests that the oxygen atom engaged in the bonding relationship with zinc oxide. The intensity of the peaks in the organic area diminished

at 2920–2856 cm^{-1} and 1708–1443 cm^{-1}, leading to a reduction in the strength of the (O-H) bond [13]. Furthermore, bands at 541 and 428 cm^{-1} were detected, ascribed to Zn–O stretching [28] - [29]. The absorption bands at 1026 cm^{-1} (C-O) and 877-1369 cm^{-1} (RCOO) were ascribed to alkaloids, flavonoids, and phenolic chemicals, respectively [30]. Following the roasting process at 450 degrees Celsius (indicated by the blue hue of ZnO NPs nanoparticles), the intensity of the peak associated with surface hydroxyl groups at 3746 cm^{-1} increased, while most organic peaks (2932, 1611, 1443 cm^{-1}) diminished or became weak due to the combustion and decomposition of organic groups. A prominent peak appeared at 540–432 cm^{-1}, corresponding to the Zn–O bond, signifying the formation of a purer and more crystalline ZnO NPs [31]. The results validated that the plant extract functioned as both a reducing and stabilizing agent throughout the green synthesis process, whereas calcination improved the purity and crystallinity of the resultant ZnO NPs [32].

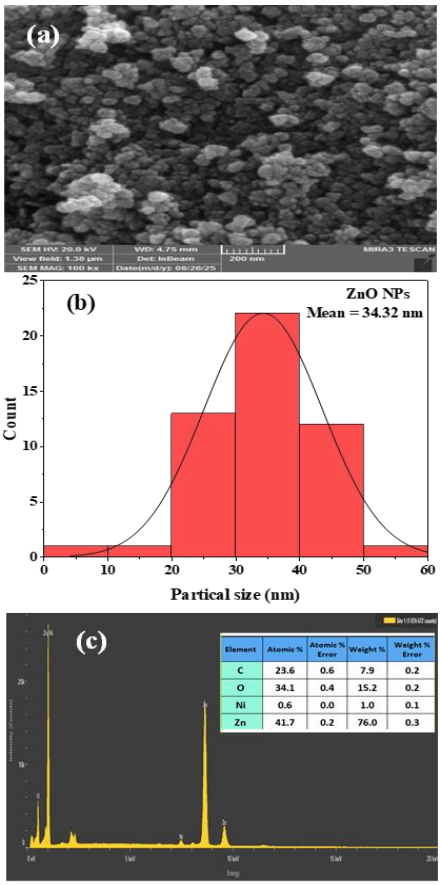

Figure 1: Shows (a-b) FESEM images depicting the and size distributions of ZnO NPs before calcination (c) The EDX spectrum of the same ZnO NPs.

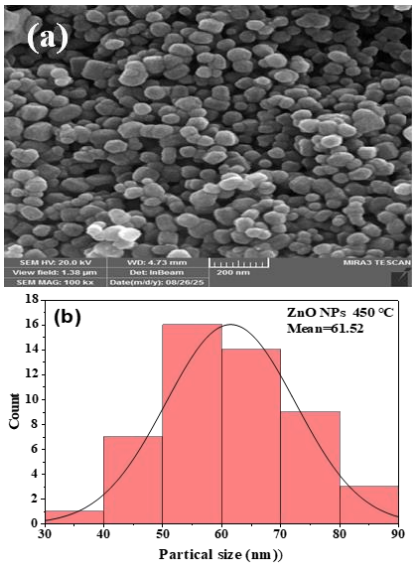

Figure 2: (a) FESEM images and (b) Particle size distributions of ZnONPs after calcination at 450 °C.

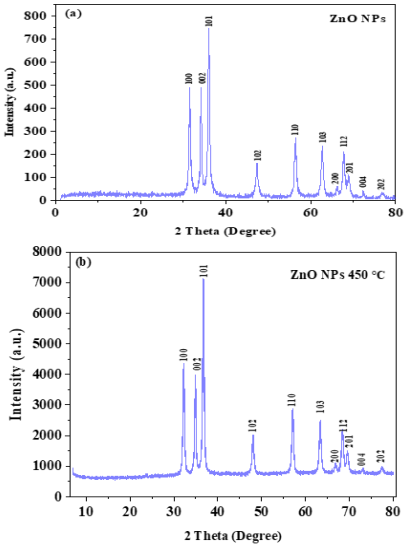

Figure 3: (a) XRD pattern of ZnONPs nanoparticles before calcination (b) XRD pattern after calcination of ZnONPs nanoparticles at 450 °C.

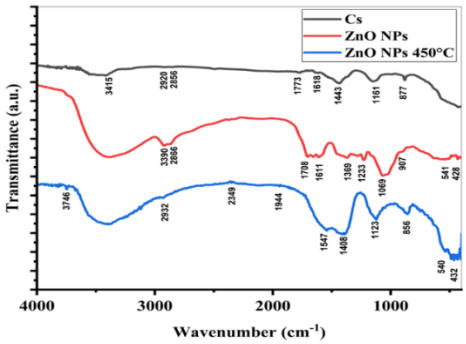

Figure 4: Displays the (FT-IR) spectra of Crocus sativus L and (ZnO NPs) before and after calcination.

3.4 UV-Visible Analyses

The optical characteristics defined by the diffuse absorption spectra of ZnO NPs nanoparticles synthesized by the green technique were examined and contrasted with those of zinc oxide calcined at 450°C; refer to Figure 5a, 5b. A solitary peak was seen with a wavelength of 274 nm. The peak can be ascribed to the phytochemicals in saffron leaf extracts (Crocus sativus L.), as it is plausible to claim that the hydroxyl groups function as numerous stabilizing agents. Nanoparticles can be synthesized using bio-reduction [14]. The spectra exhibited a peak at 345 nm, indicative of ZnO NPs nanoparticles. The absorbance peak for ZnO NPs nanoparticles is reported to be between 310 nm and 360 nm in wavelength [27], [33]. In Figure 5b upon calcination, the zinc oxide nanoparticles exhibited a prominent peak at 375 nm, ascribed to the temperature. ZnO NPs powder demonstrates significant ultraviolet absorption, a high absorbance rate below 400 nm, exceptional clarity, and a limited visible absorption spectrum when subjected to varying calcination temperatures [34]. Deficient absorption values at extended wavelengths result from defects in ZnO NPs nanoparticles, which depend on the crystal's quality, lattice parameters, crystal size, and the presence of oxygen vacancies acting as donor impurities, thus directly affecting the optical property values [35]. The energy band gap was determined using the Tauck technique [36]. As seen in Figure 6a, 6b the determination was made by examining the linear segment of the graph depicting $(\alpha hv)^2$ against photon energy (hv). The energy gap of ZnO nanoparticles prior to calcination was recorded at 2.89 eV, as seen in Figure 6a, However, when the temperature was elevated to 450 °C, the band gap rose to 3.5 eV. The modulation of band gap energy may pertain to the modification of thermal vibrations of lattice atoms and the diminution of defects, which contribute to an increase in the energy band gap [37]. The augmentation of the energy band gap signifies the occurrence of quantization events [38].

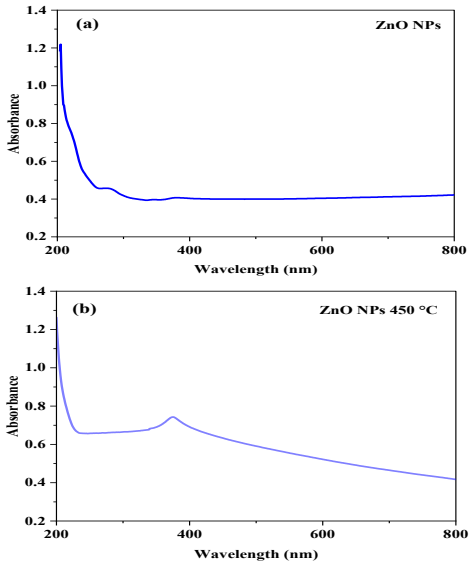

Figure 5: UV-visible spectra (a) Before calcination ZnO NPs (b) After calcination ZnO NPs.

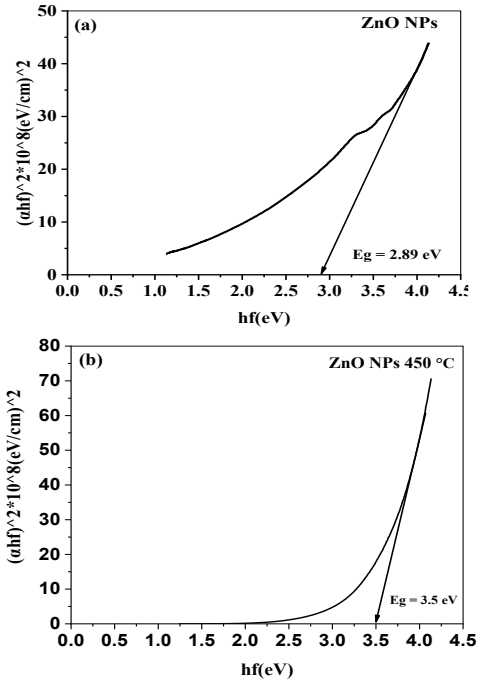

Figure 6: The energy band gap of (a) Before calcination ZnO NPs (b) After calcination ZnO NPs to 450 °C.

3 CONCLUSIONS

This paper presents a direct, economical and environmentally friendly approach to manufacturing zinc oxide using an extract of the leaves of the saffron tree (Crocus sativus L) and addresses the effect of the extract on the properties of zinc oxide nanoparticles (ZnO NPs), encompassing their crystal structure, dimensions, average size, morphology, functional groups, elemental composition. The results indicated that variations in the calcination (annealing) temperature considerably influence the characteristics of the ZnO NPs nanoparticles. significantly influences the quality and mean crystal size. The field emission scanning electron microscopy (FESEM) study indicated that the particle size before to calcination was approximately 34.32 nm, which rose to 61.52 nm following calcination at 450 °C. This rise signifies the impact of temperature on atomic rearrangement inside the nanostructure, resulting in augmented crystalline density and increased structural stability. The crystallite size determined using the Scherrer equation correlated well with the transmission electron microscopy pictures. The EDX investigations confirmed the purity and chemical composition of the zinc oxide. The UV-visible examination of ZnO NPs nanoparticles indicated a prominent peak for synthesized zinc oxide nanoparticles at a calcination temperature of 450°C, substantial absorbance in the UV area below 400 nm. Findings indicates that when the temperature was elevated the band gap rose to 3.5 eV, this signifies an enhancement in the electrical and optical characteristics of the nanoparticles post-calcination. The comprehensive analysis of the attributes of zinc oxide nanoparticles shows that calcination at 450 °C is the optimal condition for obtaining ZnO nanoparticles with more uniform crystallinity and higher optical purity. The improvements in both structural and optical properties endow the nanoparticles with enormous potential for advanced applications, including ultraviolet sensors, antibacterial coatings, and photocataltic wastewater treatment. Accordingly, this work provides a significant contribution to the development of a sustainable and cost-effective approach for synthesising functional nanomaterials from natural plant-based sources, thereby supporting the global shift towards green technologies in nanomaterial science.

REFERENCES

[1] D. H. Samak et al., “Developmental toxicity of carbon nanoparticles during embryogenesis in chicken,” Environ. Sci. Pollut. Res., vol. 27, no. 16, pp. 19058-19072, 2020, [Online]. Available: https://doi.org/10.1007/s11356-018-3675-6.

[2] M. S. Aref and S. S. Salem, “Bio-callus synthesis of silver nanoparticles, characterization, and antibacterial activities via Cinnamomum camphora callus culture,” Biocatal. Agric. Biotechnol., vol. 27, p. 101689, 2020, [Online]. Available: https://doi.org/10.1016/j.bcab.2020.101689.

[3] S. M. Alsharif et al., “Multifunctional properties of spherical silver nanoparticles fabricated by different microbial taxa,” Heliyon, vol. 6, no. 5, 2020, [Online]. Available: https://doi.org/10.1016/j.micpath.2020.104741.

[4] T. I. Shaheen, S. S. Salem, and S. Zaghloul, “A new facile strategy for multifunctional textiles development through in situ deposition of SiO_2/TiO_2 nanosols hybrid,” Ind. Eng. Chem. Res., vol. 58, no. 44, pp. 20203-20212, 2019, [Online]. Available: https://doi.org/10.1021/acs.iecr.9b04655.

[5] Abdel-Azeem, A. A. Nada, A. O’Donovan, V. K. Thakur, and A. Elkelish, “Mycogenic silver nanoparticles from endophytic Trichoderma atroviride with antimicrobial activity,” J. Renew. Mater., vol. 8, no. 2, pp. 171-185, 2020, [Online]. Available: https://doi.org/10.32604/jrm.2020.08960.

[6] L. Collenburg et al., “The activity of the neutral sphingomyelinase is important in T cell recruitment and directional migration,” Front. Immunol., vol. 8, p. 1007, 2017, [Online]. Available: https://doi.org/10.3389/fimmu.2017.01007.

[7] S. S. Salem et al., “Bactericidal and in vitro cytotoxic efficacy of silver nanoparticles (Ag-NPs) fabricated by endophytic actinomycetes and their use as coating for the textile fabrics,” Nanomaterials, vol. 10, no. 10, p. 2082, 2020, [Online]. Available: https://doi.org/10.3390/nano10102082.

[8] H. M. Yusof, R. Mohamad, U. H. Zaidan, and N. A. A. Rahman, “Microbial synthesis of zinc oxide nanoparticles and their potential application as an antimicrobial agent and a feed supplement in animal industry: a review,” J. Anim. Sci. Biotechnol., vol. 10, no. 1, p. 57, 2019, [Online]. Available: https://doi.org/10.1186/s40104-019-0368-z.

[9] W. Ahmad and D. Kalra, “Green synthesis, characterization and antimicrobial activities of ZnO nanoparticles using Euphorbia hirta leaf extract,” J. King Saud Univ.–Sci., vol. 32, no. 4, pp. 2358-2364, 2020, [Online]. Available: https://doi.org/10.1016/j.jksus.2020.03.014.

[10] S. Bettini et al., “Promising piezoelectric properties of new ZnO@octadecylamine adduct,” J. Phys. Chem. C, vol. 119, no. 34, pp. 20143-20149, 2015, [Online]. Available: https://doi.org/10.1021/acs.jpcc.5b06013.

[11] H. Hong et al., “Cancer-targeted optical imaging with fluorescent zinc oxide nanowires,” Nano Lett., vol. 11, no. 9, pp. 3744-3750, 2011, [Online]. Available: https://doi.org/10.1021/nl201782m.

[12] A. N. Abdulqudos and A. F. F. Abdulrahman, "Biosynthesis and characterization of ZnO nanoparticles by using leaf extraction of Allium calocephalum Wendelbow plant," Passer J. Basic Appl. Sci., vol. 4, no. 2, pp. 113-126, 2022, [Online]. Available: https://doi.org/10.24271/psr.2022.343112.1136.

[13] T. Gur, I. Meydan, H. Seckin, M. Bekmezci, and F. Sen, "Green synthesis, characterization and bioactivity of biogenic zinc oxide nanoparticles," Environ. Res., vol. 204, p. 111897, 2022, [Online]. Available: https://doi.org/10.1016/j.envres.2021.111897.

[14] P. Singh, Y.-J. Kim, D. Zhang, and D.-C. Yang, "Biological synthesis of nanoparticles from plants and microorganisms," Trends Biotechnol., vol. 34, no. 7, pp. 588-599, 2016, [Online]. Available: https://doi.org/10.1016/j.tibtech.2016.02.006.

[15] S. M. Ismail and S. M. Ahmed, "The effect of calcination temperatures on the properties of ZnO nanoparticles synthesized by using leaves extracts of Pinus brutia tree," Sci. J. Univ. Zakho, vol. 11, no. 2, pp. 286-297, 2023, [Online]. Available: https://doi.org/10.25271/sjuoz.2023.11.2.1087.

[16] M. B. Mobarak, M. S. Hossain, F. Chowdhury, and S. Ahmed, "Synthesis and characterization of CuO nanoparticles utilizing waste fish scale and exploitation of XRD peak profile analysis for approximating the structural parameters," Arab. J. Chem., vol. 15, no. 10, p. 104117, 2022, [Online]. Available: https://doi.org/10.1016/j.arabjc.2022.104117.

[17] M. B. Mobarak et al., "From discarded to desired: valorization of Zn–C battery waste into crystalline ZnO nanoparticles with crystallographic insights and antibacterial efficacy," RSC Adv., vol. 15, no. 46, pp. 38454-38469, 2025, [Online]. Available: https://doi.org/10.1039/D5RA06684K.

[18] R. De Silva, M. Jayaweera, V. Perera, I. Jayarathna, and S. Rosa, "Sodium nickel oxide nanoporous cathodes used for sodium-ion rechargeable batteries," Sri Lankan J. Phys., vol. 15, 2015, [Online]. Available: https://doi.org/10.4038/sljp.v15i0.8021.

[19] A. Alwash, "Impact of calcination temperature on the structural and photocatalytic properties of ZnO synthesized from gum arabic for methylene blue dye removal," J. Hazard. Mater. Adv., vol. 17, p. 100625, 2025, [Online]. Available: https://doi.org/10.1016/j.hazadv.2025.100625.

[20] S. Fakhari, M. Jamzad, and H. K. Fard, "Green synthesis of zinc oxide nanoparticles: a comparison," Green Chem. Lett. Rev., vol. 12, no. 1, pp. 19-24, 2019, [Online]. Available: https://doi.org/10.1080/17518253.2018.1547925.

[21] S.-Y. Pung, W.-P. Lee, and A. Aziz, "Kinetic study of organic dye degradation using ZnO particles with different morphologies as a photocatalyst," Int. J. Inorg. Chem., vol. 2012, p. 608183, 2012, [Online]. Available: https://doi.org/10.1155/2012/608183.

[22] R. Sathyavathi, M. B. Krishna, S. V. Rao, R. Saritha, and D. N. Rao, "Biosynthesis of silver nanoparticles using Coriandrum sativum leaf extract and their application in nonlinear optics," Adv. Sci. Lett., vol. 3, no. 2, pp. 138-143, 2010, [Online]. Available: https://doi.org/10.1166/asl.2010.1099.

[23] A. A. Barzinjy and H. H. Azeez, "Green synthesis and characterization of zinc oxide nanoparticles using Eucalyptus globulus Labill. leaf extract and zinc nitrate hexahydrate salt," SN Appl. Sci., vol. 2, no. 5, p. 991, 2020, [Online]. Available: https://doi.org/10.1007/s42452-020-2813-1.

[24] M. Abdo et al., "Green synthesis of zinc oxide nanoparticles (ZnO-NPs) by Pseudomonas aeruginosa and their activity against pathogenic microbes and common house mosquito, Culex pipiens," Materials, vol. 14, no. 22, p. 6983, 2021, [Online]. Available: https://doi.org/10.3390/ma14226983.

[25] Y.-F. Chen, C.-Y. Lee, M.-Y. Yeng, and H.-T. Chiu, "The effect of calcination temperature on the crystallinity of TiO_2 nanopowders," J. Cryst. Growth, vol. 247, no. 3-4, pp. 363-370, 2003, [Online]. Available: https://doi.org/10.1016/S0022-0248(02)01938-3.

[26] N. M. Wannas, A. A. S. Al-Hamdani, and W. Al Zoubi, "Spectroscopic characterization for new complexes with 2,2′-(5,5-dimethylcyclohexane-1,3-diylidene)bis(azan-1-yl-1-ylidene)dibenzoic acid," J. Phys. Org. Chem., vol. 33, no. 11, p. e4099, 2020, [Online]. Available: https://doi.org/10.1002/poc.4099.

[27] A. Jayachandran, T. Aswathy, and A. S. Nair, "Green synthesis and characterization of zinc oxide nanoparticles using Cayratia pedata leaf extract," Biochem. Biophys. Rep., vol. 26, p. 100995, 2021, [Online]. Available: https://doi.org/10.1016/j.bbrep.2021.100995.

[28] F. Buazar et al., "Potato extract as reducing agent and stabiliser in a facile green one-step synthesis of ZnO nanoparticles," J. Exp. Nanosci., vol. 11, no. 3, pp. 175-184, 2016, [Online]. Available: https://doi.org/10.1080/17458080.2015.1039610.

[29] C.-C. Chen et al., "Degradation of crystal violet by an FeGAC/H_2O_2 process," J. Hazard. Mater., vol. 196, pp. 420-425, 2011, [Online]. Available: https://doi.org/10.1016/j.jhazmat.2011.09.042.

[30] S. Yadav, T. Nadar, J. Lakkakula, and N. S. Wagh, "Biogenic synthesis of nanomaterials: bioactive compounds as reducing and capping agents," in Biogenic Nanomaterials for Environmental Sustainability: Principles, Practices, and Opportunities, Springer, 2024, pp. 147-188, [Online]. Available: https://doi.org/10.1007/978-3-031-45956-6_6.

[31] J. Lu et al., "Photocatalytic degradation of methylene blue using biosynthesized zinc oxide nanoparticles from bark extract of Kalopanax septemlobus," Optik, vol. 182, pp. 980-985, 2019, [Online]. Available: https://doi.org/10.1016/j.ijleo.2018.12.016.

[32] P. Ganesan and D. Narayanasamy, "Lipid nanoparticles: different preparation techniques, characterization, hurdles, and strategies for the production of solid lipid nanoparticles and nanostructured lipid carriers for oral drug delivery," Sustain. Chem. Pharm., vol. 6, pp. 37-56, 2017, [Online]. Available: https://doi.org/10.1016/j.scp.2017.07.002.

[33] R. Nayak et al., "Fabrication of CuO nanoparticle: an efficient catalyst utilized for sensing and degradation of phenol," J. Mater. Res. Technol., vol. 9, no. 5, pp. 11045-11059, 2020, [Online]. Available: https://doi.org/10.1016/j.jmrt.2020.07.100.

[34] L. Roza, M. Rahman, A. Umar, and M. M. Salleh, "Direct growth of oriented ZnO nanotubes by self-selective etching at lower temperature for photo-electrochemical solar cell application," J. Alloys Compd., vol. 618, pp. 153-158, 2015, [Online]. Available: https://doi.org/10.1016/j.jallcom.2014.08.113.

[35] R. Shabannia and H. A. Hassan, "Characteristics of photoconductive UV photodetector based on ZnO nanorods grown on polyethylene naphthalate substrate by chemical bath deposition method," Electron. Mater. Lett., vol. 10, no. 4, pp. 837-843, 2014, [Online]. Available: https://doi.org/10.1007/s13391-014-3245-0.

[36] A. F. Abdulrahman et al., "Fabrication and characterization of high-quality UV photodetectors based on ZnO nanorods using traditional and modified chemical bath deposition methods," Nanomaterials, vol. 11, no. 3, p. 677, 2021, [Online]. Available: https://doi.org/10.3390/nano11030677.

[37] S. U. Awan, S. Hasanain, G. Hassnain Jaffari, D. H. Anjum, and U. S. Qurashi, "Defects induced luminescence and tuning of bandgap energy narrowing in ZnO nanoparticles doped with Li ions," Journal of Applied Physics, vol. 116, no. 8, 2014, [Online]. Available: https://doi.org/10.1063/1.4894153.

[38] S. Mandal, S. I. Ali, S. Pramanik, and A. C. Mandal, "Impact of capping agent on structural and optical properties of ZnS nanoparticles," arXiv preprint arXiv:2304.13420, 2023, [Online]. Available: https://doi.org/10.48550/arXiv.2304.13420.